Maleic Anhydride Polypropylene Modified Cellulose Nanofibril Polypropylene Nanocomposites With Enhanced Impact Strength

Yucheng Peng,[1] Sergio A. Gallegos,[2] Douglas J. Gardner,[3,4] Yousoo Han,[3,4] Zhiyong Cai[5]
[1]*Department of Materials Science and Engineering, Clemson University, Clemson, South Carolina 29634*

[2]*Chemical Engineering, Universidad de Concepción, Avenida Cordillera 2634-Parque Industrial Coronel, Coronel, Chile*

[3]*Advanced Structures and Composites Center, University of Maine, Orono, Maine 04469*

[4]*School of Forest Resources, University of Maine, Orono, Maine 04469*

[5]*Forest Products Laboratory, USDA Forest Service, Madison, Wisconsin 53726-2398*

Development of cellulose nanofibrils (CNFs) reinforced polypropylene (PP) nanocomposites using melt compounding processes has received considerable attention. The main challenges are to obtain well-dispersed CNFs in the polymer matrix and to establish compatible linkages between the CNFs and PP. Manufacturing of CNF reinforced PP nanocomposites was conducted using a twin-screw co-rotating extruder with the masterbatch concept. Modifications of CNFs using maleic anhydride polypropylene were performed. The best mechanical properties of the nanocomposites are 1.94 GPa (tensile modulus), 32.8 MPa (tensile strength), 1.63 GPa (flexural modulus), 50.1 MPa (flexural strength), and 3.8 kJ m^{-2} (impact strength), which represents about 36, 11, 21, 7, and 23% improvement, respectively, compared to those of pure PP (1.43 GPa, 29.5 MPa, 1.35 GPa, 46.9 MPa, and 3.1 kJ m^{-2}). Fracture morphology examination indicated good dispersion of CNFs in the PP matrix was achieved through this specific manufacturing process. MAPP treatments enhanced the interfacial adhesion between the CNFs and PP. POLYM. COMPOS., 00:000–000, 2014. © 2014 Society of Plastics Engineers

INTRODUCTION

The unique aspect of polymer composites reinforced by various fillers or additives is that the mechanical properties of the material can be tailored to fit a variety of uses: construction, transportation, industrial, and consumer applications. By selecting a specific reinforcement or designing a particular manufacturing process a material with desired properties can be achieved. In recent years, interest in composites reinforced by renewable materials (wood flour/cellulose fibers) has grown tremendously because of social requests for low environmental impact (biodegradable materials), low-maintenance, and high-durability products [1]. Cellulose, one of the basic structural components of wood fibers, is the most abundant polymer on earth and has a great potential for the preparation of novel composite materials with thermoplastic resins [2, 3]. When compared to conventional reinforcements such as glass fibers or inorganic fillers, cellulosic materials offer a series of advantages: lower density (1.5 g cm^{-3}), better recyclability and disposal, lower price, reduced abrasion to processing machinery, carbon neutrality, and modifiable surface properties [4–6].

Various cellulosic reinforcements have been used in reinforcing polymers: wood fibers, paper fibers, pulp fibers, rice-husk flour, flax, jute, sisal, microcrystalline cellulose (MCC), cellulose nanofibrils (CNFs), and cellulose nanocrystals (CNCs) [2, 6–11]. Among them, cellulose nanofibrils and cellulose nanocrystals are the elementary fibrils of cellulose materials, e.g. cellulose nanofibers. With high stiffness and strength, cellulose nanofiber as a reinforcing component in polymer composites has been studied intensively [11–19]. As cellulose nanofibers are available from pilot-scale production facilities in the US, Europe, Canada, and Japan [20–22], a

Correspondence to: Y. Peng; e-mail: yucheng@clemson.edu
Contract grant sponsor: Maine Agricultural and Forestry Experiment Station Mclntire-Stennis Project; contract grant number: ME0-M-8-00527-13.
DOI 10.1002/pc.23235
Published online in Wiley Online Library (wileyonlinelibrary.com).
© 2014 Society of Plastics Engineers

renewable nano-scale material from forest products can be practically utilized in manufacturing bio composites, innovative bio plastics, and advanced reinforced composite materials. Selection of the polymer matrix for utilization in reinforced polymer composites is also important. Among the commodity plastics, polypropylene (PP) is widely used because of its low price, light weight, good weatherability, design flexibility, recyclability, and its attractive combination of good processability, mechanical properties, and chemical resistance [2, 23]. Commercially available PP is produced in a wide variety of molecular weights with the melt flow indices (MFI) ranging from 0.3 to more than 1000 g/10 min [24]. Reinforced by filler or fiber, PP can be used instead of other commodity thermoplastics and even engineering thermoplastics such as polycarbonate (PC) and acrylonitrile butadiene styrene (ABS) [25]. Reinforced PP composites can be produced using various processing techniques including injection molding, compression molding, blow molding, extrusion, and thermoforming. Recent developments in filled-PP composites show that high performance materials can be obtained by reinforcing PP using environmentally friendly reinforcements (wood fibers/cellulose fibers) [1, 2, 26, 27]. CNFs have also been used in reinforcing PP. Adding CNFs in PP was observed to improve the mechanical properties and thermostability of PP [2, 10, 28]. These advantages of PP and the research on filled-PP composites provide the basis to develop improved CNF-reinforced PP nanocomposites.

Melt compounding is the most common method used to create thermoplastic polymer nanocomposites. It is considered to be cost-effective, flexible for formulation, and involves compounding and fabrication facilities commonly used in commercial practice, such as extrusion, injection molding, compression molding, etc. [29]. However, melt compounding is less effective at dispersing nanofillers and is limited to low nanofiller loadings because of the high viscosity of the nanocomposites caused by the addition of nanofillers [29]. As a general rule of thumb, the better the nanofiller dispersion, the better the properties of the final nanocomposite. Nanofillers, in essence, agglomerate based on their high specific surface area and high surface energy, and it is very difficult to disperse them in relatively low surface energy polymer matrices, such as PP. The hydrophilic nature of cellulose nanofibers [30, 31] causes serious agglomeration during direct mixing with the polymer matrix, even in the process of mixing with polar polymer matrices. Cellulose nanocrystal suspensions were directly compounded with polar polymers of starch [32] and poly(oxyethylene) (PEO) [33] using an extrusion process. Pre-mixing of cellulose nanocrystal suspension with the polymer solutions was conducted prior to extrusion. Agglomeration or poor dispersion of the cellulose nanocrystals within polymer matrices was observed [32, 33]. CNF suspensions were also directly added into apolar PP [2] and polylactic acid (PLA) [34] during the melt compounding process. Serious CNF agglomeration in the polymers occurred. Several strategies have been developed to improve the dispersion quality of cellulose nanofibers in polymers before or during melt compounding process: (1) pre-mixing of the cellulose nanofiber suspension with polymer using organic solvents as the medium prior to extrusion [34–36]; (2) generation of highly loaded cellulose nanofiber masterbatch in polymers using organic solvents before extrusion [37]; (3) pre-treatment of polymers using processing aids during extrusion to decrease viscosity [38]; (4) production of a carrier system for cellulose nanofibers using a different polymer matrix before extrusion [39]; (5) improvement of the compatibility between cellulose nanofibers and polymers using coupling agents [40–42]; (6) grafting of chemicals or polymer molecules onto the surface of cellulose nanofibers [43, 44]; and (7) drying cellulose nanofibers while maintaining their nano-scale dimensions [3, 45]. Among them, strategies of (1), (2), and (6) use organic solvents. Strategy (3) needs to consider the compatibility between the carrier polymer and the substrate matrix. These strategies induce an extra step, are time-consuming and not compatible with the industrial practices for producing thermoplastic nanocomposites. Drying cellulose nanofibers while maintaining their nano-scale dimensions has been studied in detail and the dry form of cellulose nanofibers can be produced by the spray-drying process [3, 45]. Therefore, drying cellulose nanofibers and then compounding cellulose nanofibers in a dry form with polymer melts through the extrusion process is recommended. The strategies of using processing aids or compatibilizers during the extrusion process can also be helpful. Simultaneously, using processing aids or compatibilizers solves the incompatibility problem encountered in cellulose nanofibers-reinforced PP nanocomposites. This incompatibility is mainly caused by the high density of hydroxyl groups on the cellulose nanofiber surface and was observed to seriously degrade the mechanical properties of the final composites [4, 8].

To avoid the drawbacks induced by the surface hydroxyl groups in the melt compounding process, the cellulose fiber can be subjected to specific surface modification to (1) decrease agglomeration during drying, (2) provide an efficient hydrophobic barrier, and (3) minimize interfacial energy with the nonpolar polymer matrix and thus generate optimum adhesion. Further improvement in interfacial strength, which is a basic requirement for the mechanical performance of any composite, is attained by chain entanglement between the matrix macromolecules and long chains appended to the fiber surface. The hydroxyl groups on the cellulose nanofiber surface can be modified using a series treatments, such as silane treatments [46, 47], esterification [37, 48], alkaline treatment [49], maleic anhydride-grafted polypropylene (MAPP) treatment [26, 27, 50], and others [50–52]. For the specific cellulose/polypropylene system, coupling agent treatment using MAPP has been found to be one of the most efficient ways in improving the mechanical properties of cellulose composite materials [1, 26, 27, 53].

 DOI 10.1002/pc

The overall goal of this study was to develop cellulose nanofibril (CNF)-reinforced PP nanocomposites using melt compounding processes. This can be subdivided into two specific objectives: (1) achieve well-dispersed CNFs in the PP matrix and (2) obtain enhanced compatibility between the CNFs and PP. CNFs were first obtained by spray-drying and were then incorporated into the PP matrix by two steps. The concept of masterbatch mixing was employed. A masterbatch of highly loaded CNFs in PP was prepared as the first step and then the masterbatch was diluted using fresh PP to manufacture the nanocomposites with the final loading of CNFs using a twin-screw co-rotating extruder. The effect of using MAPP as a coupling agent on the mechanical properties of CNF-reinforced PP nanocomposites was also investigated. Two strategies were employed for the utilization of MAPP coupling agents. *In situ* modification of the CNF suspension using MAPP emulsion treatment during the spray-drying process was performed as the first method. Then the treated CNFs were used to manufacture nanocomposites. The second method is to add MAPP in pellet form into the masterbatch during masterbatch compounding process. A masterbatch of CNFs in a mixture of MAPP and PP pellets was first prepared and then was diluted using pure PP with a twin-screw extrusion process. An injection molder was used finally to produce the nanocomposite samples for mechanical testing, including tensile, flexural, and impact tests. The effects of the two strategies of using MAPP treatment and the dispersion of CNFs in the polymer matrix on the mechanical properties were evaluated.

EXPERIMENTAL

Materials

Homopolymer PP (H05A-99) with the density of 0.89–0.93 g cm^{-3} was supplied by INEOS Olefins & Polymers USA (League City, TX). The 3 wt% CNF suspension was provided by the Chemical Engineering Department at the University of Maine.

Maleic anhydride modified homopolymer polypropylene (MAPP) pellets (Polybond 3200) and a nonionic polypropylene emulsion (MAPP emulsion of FGLASS™ X35) were provided by Chemtura Corporation (Lawrenceville, GA) and Michelman (Cincinnati, OH), respectively. The specific gravity and the solids content of the main non-volatile (maleated polypropylene) for the emulsion are 0.96–0.98 g cm^{-3} and 34–36 wt%. The maleic anhydride level in Polybond 3200 pellets is about 1.0 wt%. The melting point and density of Polybond 3200 is 157°C and 0.91 g cm^{-3}. The melt flow at 190°C at a load of 2.16 kg is 115 g/10 min.

Drying of the CNF Suspensions

Drying of the CNF suspensions was conducted using a Buchi B-290 laboratory spray dryer (New Castle, DE). The spray-drying process is detailed in Peng et al. [3] and Peng et al. [45]. In this study, a 1 wt% CNF suspension was dried at an inlet temperature of 200°C, gas flow rate of 601 l h^{-1}, pump rate of 9 ml min^{-1}, and drying gas flow rate of ~35 m^3 h^{-1}. For the emulsion treatment of the CNF suspension, the MAPP emulsion was added to the 1 wt% CNF suspension at a weight ratio of CNF to MAPP of 3:1 and then mixed using a Speed Mixer® (Flack Tek, US) for 2 min at 2000 rpm, followed by ultrasonic treatment at 80°C for 1 h. The emulsion treated suspension was then dried using the same spray-drying process. The MAPP emulsion treated CNFs is denoted as MAPP_CNF. The outlet temperatures of spray-dryer measured for both untreated and treated samples were around 85–88°C. All the dried CNFs were put in plastic bags and stored in a desiccator at ambient temperature for future use.

Particle Size Analysis

The particle size distributions (PSDs) of CNFs in suspension and dry form were determined using a Mastersizer 2000 particle size analyzer (Malvern Instruments, Malvern, UK), for dry samples analysis using the Sirocco 2000 dry dispersion unit and for suspension samples analysis using the Hydro 2000S unit. The PSD of CNFs in suspension with and without MAPP emulsion was measured first. After ultrasonic treatment, the PSD of the mixture was measured again to evaluate its effect. The measurements on dry CNFs were taken at four-bar of air pressure and 20% of feeder capacity. For the measurement of suspension samples, pump rate at 2100 rpm and sonication at 20% of the sonication capacity were employed. Five replicates were measured for each sample.

Composite Manufacturing

The CNF-reinforced PP nanocomposites were manufactured in two steps. Three masterbatches with 30 wt% CNF loading were first prepared according to the masterbatch formulations shown in Table 1. Then these masterbatches were diluted using fresh PP to the final loading of CNFs lzaccording to the composite formulations in Table 1.

The three masterbatches were manufactured using a C. W. Brabender Prep Mixer® (C. W. Brabender Instruments, South Hackensack, NJ). Prior to compounding, the PP pellets, MAPP pellets, and spray-dried CNFs (treated and untreated) were dried in an oven at 105°C for 2 h. Polymer pellets (PP or PP and MAPP pellets) were initially melted at 200°C and then compounded with the corresponding weight of CNFs or treated CNFs (MAPP_CNF) in the Brabender for about 8–10 min at 200°C with the mixing element rotating at a speed of 60 rpm. The resulting compound was cooled and then ground in Hellweg MDS 120/150 granulator (Hackensack, NJ).

The CNF-reinforced PP nanocomposites were manufactured by diluting the 30 wt% CNF masterbatch to a

TABLE 1. Materbatch and nanocomposite formulations (wt%).

Masterbatch	PP	CNFs (dry)	MAPP pellets	MAPP solid in emulsion
PP+CNF	70	30	0	0
PP+MAPP+CNF	60	30	10	0
PP+MAPP_CNF	60	30	0	10

Composite	PP	CNFs (dry)	MAPP pellets	MAPP solid in emulsion
PP control	100	0	0	0
PP+CNF	94	6	0	0
PP+MAPP+CNF	92	6	2	0
PP+MAPP_CNF	92	6	0	2

final loading of 6 wt% with fresh PP pellets using an extrusion process. The ground masterbatch pellets were dry-mixed with PP pellets using a Speed Mixer® (Flack Tek, US) for 2 min at 2,000 rpm. Then the pellet mixture was extruded at 60 rpm through a C. W. Brabender 20 mm Clamshell Segmented Twin-Screw Co-rotating Extruder attached to an Intelli-Torque Plastic-Corder drive system (C. W. Brabender Instruments, South Hackensack, NJ). The pellet mixture was fed into the first zone of the extruder through the feed hopper at about 70 g min^{-1}. The screw configuration of the system is a stand-alone TSE20/40D. The five heating zones were set at 200°C. The composite extrudate passed through a two-nozzle die having a nozzle diameter of 2.7 mm. The die temperature was maintained at 200°C. The extrudate, in the melt state, was cooled and solidified directly in an air-cooling system while being pulled with a 2200 Series End Drive Conveyor from Dorner (Hartland, WI). The solidified extrudate was pelletized through a C. W. Brabender Instruments, pelletizer. The pelletized composite material was then injection molded into shapes specified by ASTM D638 and D790 for tensile, flexural and Izod impact testing. An injection molder Model #50 "Minijector" with a ram pressure of 2,500 psi at 200°C was used to produce samples. The molded samples were kept in the mold for 10 s to cool. The samples were then put into plastic containers and stored in desiccators to maintain dryness. The obtained CNF-PP nanocomposites are denoted as PP+CNF, PP+MAPP_CNF, and PP+MAPP+CNF for neat CNF, MAPP emulsion treated CNF, and MAPP pellet treated CNF reinforced PP. The as-received PP pellets went through the same extrusion and injection molding process for manufacturing the control.

Mechanical Property Tests

Tensile, flexural, and impact tests were performed according to ASTM D 638-10, ASTM D 790-10, and ASTM D 256-10 standards. Tests were conducted in an environmentally conditioned room at 23°C ± 2°C and 50% ± 5% RH. Tensile tests were performed on a servo hydraulic testing machine (Instron 5966) with a 10000-N load cell. Flexural tests were conducted with a 266.9-N load cell attached to Instron 8872. The outer fiber strain rates for tensile and flexural tests were 0.1 and 0.01 min^{-1}. Izod impact tests were performed on composite samples using a Ceast pendulum impact tester (Model Resil 50B). At least five replicates of each sample formulation were tested for the tensile and flexural properties determination. The impact test was applied to 10 replicates for each formulation. The average value of impact strength in kJ m^{-2} and standard deviation were reported. Statistical comparisons of the mechanical properties were conducted at a 0.05 significance level.

Thermogravimetric Analysis (TGA)

Thermal properties of the dried CNFs were characterized using a Mettler Toledo System consisting of the STARe Software and the TGA/SDTA851e module. All tests were performed in a nitrogen atmosphere with a ceramic sample pan. Analysis of individual sample weighing 5–15 mg was carried out at a constant heating rate of 10°C min^{-1} between 25 to 600°C. Each sample was tested in triplicate. The MAPP solid obtained by drying the emulsion to constant weight at 88°C (The outlet temperature of spray-drying of CNF suspension ranged from 85 to 88°C) was analyzed using the same procedures.

Melt Flow Index (MFI)

The melt flow index of all the composite samples was measured using the Dynisco Melt Flow Indexer Model 4004 (Morgantown, PA). The measurements were conducted at 230°C with the weight of 2.16 kg. The extrudate cut-off time-interval was set up as one minute for all samples. Five extrudate replicates were collected for each sample and weighed to the nearest 1 mg. The standard melt flow rate number with the units of g/10 min was reported.

Scanning Electron Microscopy (SEM)

The morphologies of the spray-dried CNFs and the fractured composite samples were examined by SEM using a Hitachi Tabletop Microscope SEM TM 3000 (Hitachi High-Technologies Corporation, Tokyo, Japan) at an accelerating voltage of 15 kV.

RESULTS AND DISCUSSION

Characterization of the CNFs in Suspension and in Dry Form

The PSDs of CNFs in suspension based on volume are shown in Fig. 1. In laser diffraction, the diameters of spherical materials, which generate intensity patterns of

DOI 10.1002/pc

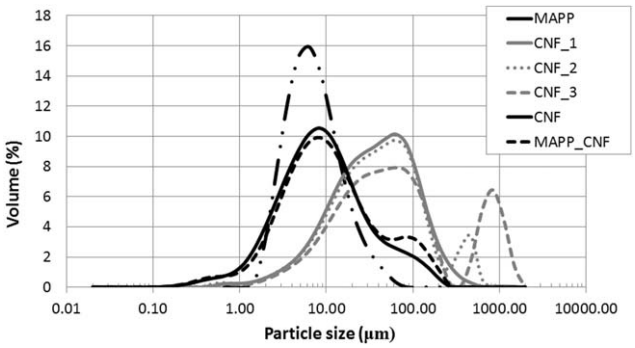

FIG. 1. Particle size distributions (PSD) of CNFs in suspension or dry form. CNF represents the PSD of spray-dried CNF. MAPP_CNF represents the PSD of spray-dried CNFs treated by MAPP emulsion. CNF_1 represents the original PSD of CNFs in suspension. CNF_2 represents the PSD of the mixture of CNFs and MAPP emulsion before ultrasonic treatment. CNF_3 represents the PSD of the mixture of CNFs and MAPP emulsion after ultrasonic treatment. MAPP indicates the PSD of solid content in MAPP emulsion.

the measured samples are characterized as the particle sizes of the measured materials (spherical equivalent diameter). A single peak with a particle size from 0.6 to 2000 μm was observed for CNF in original suspension (CNF_1). The standard percentile readings D (n, 0.1), D (n, 0.5), and D (n, 0.9) of particle sizes derived from the statistics of the distribution are 8.9, 43, and 152 μm, e.g. 50% of the CNFs by volume in suspension are smaller than 43 μm. The particle sizes of maleated polypropylene in MAPP emulsion ranged from 1.5 to 84 μm (MAPP in Fig. 1). Adding MAPP emulsion increased the particle size of the CNFs in suspension. A second peak containing about 7.7% of CNFs by volume with particle sizes from about 267 to 843 μm was observed (CNF_2). Following the ultrasonic treatment, the particle size distribution of the emulsion treated CNF (CNF_3) suspension changed again. The second peak observed before the ultrasonic treatment shifted to a larger particle size ranging from 356 to 2000 μm. The volume of the particles in this size range also increased from 7.7% to about 19.4%. Under the experimental conditions, the particle size of CNFs in suspension was increased by adding MAPP emulsion. Interaction between MAPP and CNFs might be one of the possibilities for this observation.

The PSDs of the dried CNFs (CNF in Fig. 1) are shown as black lines in Fig. 1. The particle sizes of dried CNFs ranges from 0.1 to 267 μm with standard percentile readings D (n, 0.1), D (n, 0.5), and D (n, 0.9) of 2.4, 10, and 55 μm, respectively. Compared to the CNFs in suspension, the particle sizes of dried CNFs are significantly smaller and the particle size distribution is narrower. Exclusion of the larger size of CNFs from suspension was observed. Many CNFs were deposited on the drying chamber wall. The smallest particles decreased from 0.6 μm in suspension to 0.1 μm in the dry form. The drying process may fold the longer soft CNFs in suspension [45], forming smaller or different shaped particles which generate smaller sizes during the laser diffraction measurements. The sample of MAPP_CNF showed similar particle size distributions with neat CNFs except a greater proportion of relatively larger particle sizes ranging from 84 to 267 μm (Fig. 1). As a result, the standard percentile readings for D (n, 0.1) and D (n, 0.5) were slightly greater than that of the neat CNFs with values of 2.7 and 11 μm while the value of D (n, 0.9) shift to a greater number of 85 μm. The SEM micrographs of the dried CNFs are shown in Fig. 2. Several different particle morphologies are observed: fibrous materials with different diameters and length, ribbon-like (or platelet) materials with different thicknesses, width, or length, and irregular shaped particles with different degrees of agglomeration. The detailed information on differences in spray-dried CNF morphologies is reported in Peng et al. [45]. After drying, MAPP emulsion treatment did not change the morphology of CNFs (Fig. 2b) significantly.

The TGA curves and the first derivative curves of the TGA Curves (DTG) of the dried CNFs (treated and untreated) are shown in Fig. 3. The thermal performance of spray-dried neat CNFs was studied in detail and can be divided into three regions from 25 to 600°C [54]. In region I, a small amount of mass loss was observed at temperatures below about 130°C because of the

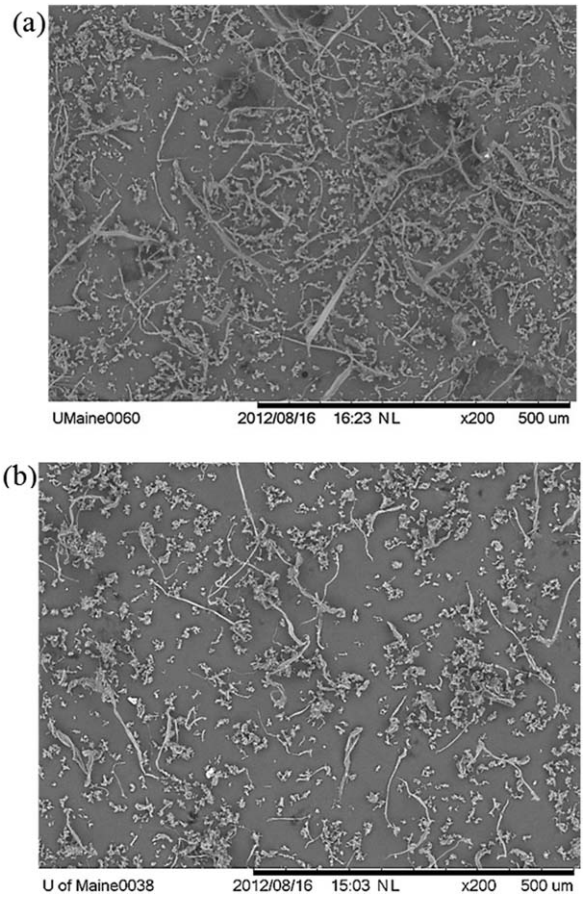

FIG. 2. SEM micrographs of spray-dried CNFs: (a) untreated and (b) MAPP emulsion treated.

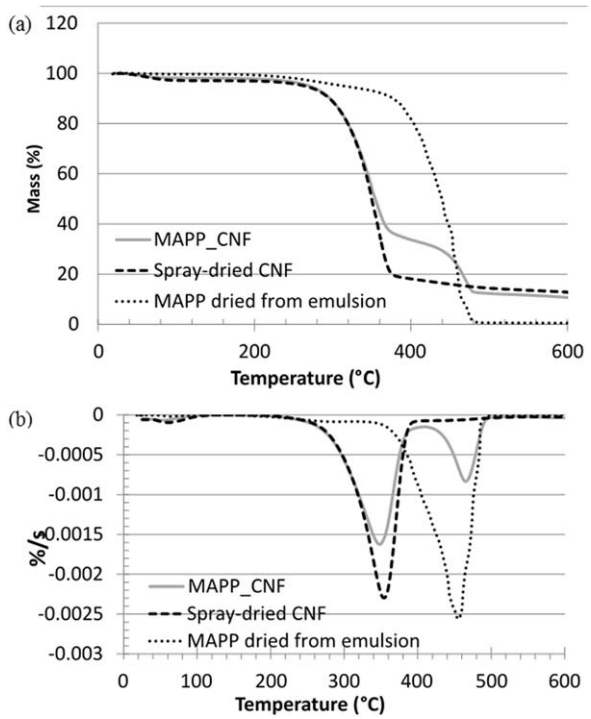

FIG. 3. TGA (a) and DTG (b) curves of dried CNFs and oven-dried MAPP emulsion.

evaporation of absorbed moisture. The moisture content of the neat CNFs (wet base) is about 2.9 wt% ± 0.1 wt%. In region II, a peak at temperature of 356°C in the DTG curve of the neat CNFs (Fig. 3b) indicates the point of greatest mass loss rate of the sample. The final mass residue of the neat CNFs at 600°C is about 13wt% ± 1.3 wt% of original mass. Slight mass loss was observed below temperatures 225°C for the dried MAPP emulsion and the moisture content was calculated as ~0.5 wt% (Fig. 3). A peak showing the maximum mass loss rate of the dried MAPP emulsion was observed at temperature of about 453°C on the DTG curve (Fig. 3b). At 600°C, the final mass of the dried MAPP emulsion was about 0.4 wt% ± 0.1 wt% of the original mass. These TGA and DTG curves of MAPP_CNF differ from those of neat CNFs and dried MAPP emulsion. Four regions can be easily divided for the TGA curves of MAPP emulsion treated CNFs. The first region still shows the effect of the absorbed moisture. The spray-dried MAPP_CNF has a moisture content of about 1.8 wt% ± 0.2 wt%, slightly lower than the neat CNFs (2.9 wt% ± 0.1 wt%). Attachment of MAPP molecules onto CNFs might be the reason for the decreased moisture content because the dried MAPP emulsion has a negligible moisture content of about 0.5 wt%. The following two regions (II and III) in the TGA and DTG curves of MAPP_CNF indicated the combined thermal behavior of neat CNFs and dried MAPP. Two peaks were observed on the DTG curve of the spray-dried MAPP_CNF. The first peak at about 347°C indicates the greatest rate of change on the sample mass for CNFs in MAPP_CNF, which is 9° lower than that of neat CNFs. The second peak at about 463°C represents the point of the greatest mass loss rate of the dried MAPP in the sample of MAPP_CNF. This temperature is about 10° higher than that of the dried MAPP emulsion (453°C). Interaction between MAPP and CNFs must be the explanation for this observed thermal behavior.

During the TGA measurement, each sample was tested in triplicate. The obtained three TGA curves were highly consistent for the MAPP emulsion treated CNFs, indicating that MAPP was uniformly incorporated into CNFs. Based on the assumption that the final mass residues for neat CNFs and the dried MAPP in MAPP_CNF were not significantly different from those corresponding individuals, the MAPP content in MAPP_CNF can be calculated according to the final mass residues shown in the TGA tests. The calculated MAPP content in MAPP_CNF is about 17 wt%, which is lower than the designed value (25 wt%) shown in the formulation in Table 1. This could be caused by the loss of MAPP during the treatment and spray-drying process. Larger particle size of MAPP_CNFs were formed and might contain higher MAPP content than that included in the smaller sized MAPP_CNF samples. During the spray-drying process, larger size of MAPP_CNF could deposit on the drying chamber wall, resulting in the lower MAPP content on the collected MAPP_CNF samples.

Mechanical Characterization of the CNF-PP Nanocomposites

The tensile modulus (modulus of elasticity, MOE), tensile strength and their statistical comparison for all the nanocomposites are shown in Fig. 4 and Table 2. PP has a tensile modulus and tensile strength of 1.43 GPa and 29.5 MPa, which are lower than the values of the CNF-PP nanocomposites. Under tensile load, PP sample responds with an initial elastic deformation, followed quickly by a viscoelastic part, where the stress gradually increases to reach a maximum at the yield point. After the yield point, continued deformation results in necking and propagation of the neck along the sample length. The stress decreases towards a plateau value with the occurrence of cold drawing until the specimen fails. The tensile modulus of PP was calculated using the elastic behavior during the tensile test while the tensile strength was derived from the yield point. The tensile deformation observed in CNF-reinforced PP differs from pure PP. The tensile strains at the maximum load of all the composites also decreased as shown in Table 2. The addition of CNFs (treated and untreated) significantly decreased the tensile strain at the maximum load. With the addition of CNFs into the PP at 6 wt% (The sample denoted as PP+CNF in Table 2), the tensile modulus and tensile strength of the composites increased to 1.71 GPa and 30.4 MPa, which corresponds to an improvement of about 20% in modulus and 3% in strength compared to pure PP. At the same time, the tensile strain at maximum load decreased from 9.2 to 6.4% (Table 2),

 DOI 10.1002/pc

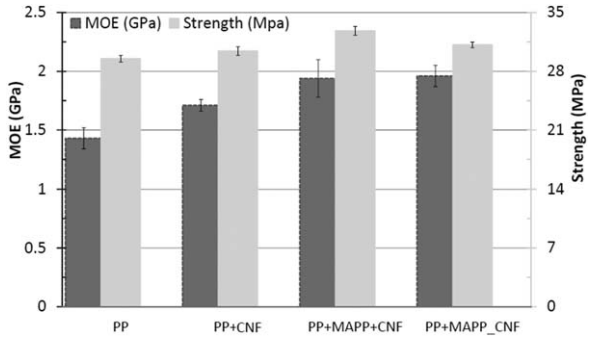

FIG. 4. The tensile properties of the PP composites.

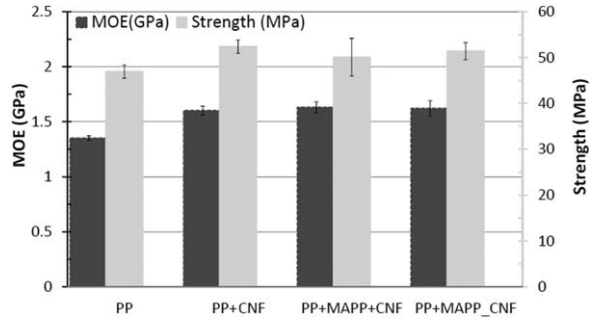

FIG. 5. The flexural properties of the PP composites.

indicating more brittle failure of PP+CNF than PP. Addition of CNFs treated by MAPP (either emulsion or pellet) into pure PP resulted in composites with higher tensile modulus and tensile strengths (Table 2). The tensile modulus (1.96 GPa) of PP reinforced by CNFs treated with MAPP emulsion (The sample denoted as PP+MAPP_CNF) is about 37% higher than that of pure PP (1.43 GPa) and the composite produced by addition of MAPP pellets into the PP/CNFs system (The sample denoted as PP+MAPP+CNF) exhibited a 36% higher tensile modulus (1.94 GPa) than that of PP. Simultaneously, the tensile strain at the maximum load decreased from 9.2% for PP to 6.1% for PP+MAPP_CNF and 6.7% for PP+MAPP+CNF, respectively (Table 2). With the addition of the stiffer CNFs in PP, the composite modulus improved. On the molecular level, the motion of PP molecules in the CNF-reinforced PP composites was restricted by the CNFs, resulting in higher stress at the elastic stage of the tensile test compared to the stress in pure PP. Therefore, the tensile modulus was improved. It is worth noting that MAPP treatment, which was used to increase the interfacial adhesion between CNFs and PP, significantly improved the tensile modulus when compared to neat CNF-reinforced PP nanocomposites (Table 2). This phenomenon is seldom observed in reinforced polymer composites [55]. The tensile modulus is measured within the elastic deformation area at a small amount of strain. There is insufficient deformation to cause interfacial separation in the elastic range. The increased interfacial bonding between CNFs and PP may not be able to improve the tensile modulus. Therefore, for PP reinforced by MAPP emulsion treated CNFs, the higher tensile modulus could be caused by: (1) the higher content of CNFs in the spray-dried sample of MAPP_CNF, and (2) the different particle size distribution of MAPP treated CNFs versus neat CNFs. In the sample of spray-dried MAPP_CNF, the MAPP content (17 wt%) is lower than the designed value (25 wt%) as indicated by the TGA analysis. Under this circumstance, the CNF content in the MAPP_CNF is higher, resulting in higher weight percentage of CNFs in the final composite. The modulus of reinforced composites consistently increases with increasing content of reinforcement [55]. For the MAPP pellet treatment, the compatibility between CNFs and PP was enhanced, facilitating the even dispersion of CNFs in PP. As a result, the tensile modulus was improved. The tensile strength of the nanocomposite PP+MAPP_CNF is 31.2 MPa, which is about 6% higher than that of pure PP (29.5 MPa) (Table 2). At the same time, the tensile strength of PP reinforced by MAPP emulsion treated CNFs is significantly higher than that of neat CNF-reinforced PP. The tensile strength of the composite is defined as the yielding stress that the composite can sustain under uniaxial tensile loading. With the introduction of the MAPP coupling agent, the compatibility between PP and CNFs is improved, resulting in increased yielding stress. The highest tensile strength was obtained by reinforcing PP with MAPP pellet treated CNFs (32.8 MPa), which is about 11% higher than that of pure PP (29.5 MPa) and, at the same time, is significantly higher than that of PP reinforced by MAPP emulsion treated CNFs.

TABLE 2. The mechanical properties of the PP composites.

Composite	Tensile properties						Flexural properties			Impact strength ($kJ\ m^{-2}$)		Melt flow index (g/10 min)
	MOE[a] (GPa)		Strength (MPa)		Strain (%)		MOE (GPa)	Strength (MPa)				
PP	1.43 ± 0.09[b]	C[c]	29.5 ± 0.4	D	9.2 ± 0.3	A	1.35 ± 0.02	46.9 ± 1.4	B	3.1 ± 0.6	B	7.2 ± 0.2
PP+CNF	1.71 ± 0.05	B	30.4 ± 0.5	C	6.4 ± 0.2	B	1.60 ± 0.04	52.4 ± 1.4	A	3.0 ± 0.4	B	8.7 ± 0.4
PP+MAPP_CNF	1.96 ± 0.09	A	31.2 ± 0.3	B	6.1 ± 0.3	C	1.62 ± 0.07	51.4 ± 1.9	A	3.0 ± 0.4	B	7.8 ± 0.4
PP+MAPP+CNF	1.94 ± 0.16	A	32.8 ± 0.5	A	6.7 ± 0.5	B	1.63 ± 0.05	50.1 ± 4.1	A	3.8 ± 0.3	A	7.4 ± 0.4

[a]Modulus of elasticity.
[b]Standard deviation.
[c]The letters A, B, C, and D represent the significant levels in statistical analysis. The values with different letters are significantly different.

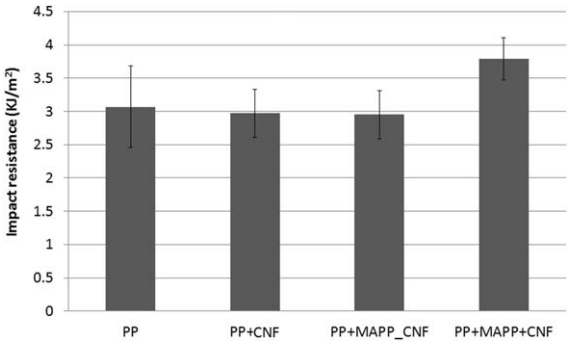

FIG. 6. The impact strength of the PP composites.

The flexural properties of all the composites are shown in Table 2 and Fig. 5. During the flexure tests, all the composites did not yield or break within a 5% strain limit. The reported strength data in Table 2 and Fig. 5 are calculated based on the 5% strain limit. The lowest flexural modulus and flexural strength is pure PP with the values of 1.35 GPa and 46.9 MPa. All the other composites with addition of CNFs showed significant improvement in flexural modulus and flexural strength (Table 2). Adding neat CNFs in pure PP significantly improved the flexural modulus to 1.60 GPa and flexural strength to 52.4 MPa. MAPP treatment on CNFs did not change the flexural modulus or strength significantly compared with the neat CNF-reinforced PP (Table 2). The highest flexural modulus and flexural strengths were 1.63 GPa and 52.4 MPa for the CNF-reinforced PP, which represents about 21 and 12% improvement when compared to pure PP. Flexural behavior of the composites differed from the tensile performance. The flexural properties are a combination of tensile and compression behaviors. Additionally, the mechanical properties of homopolymer polypropylenes and its filled composites are greatly influenced by strain rate [56]. In this test, flexural tests were conducted at an outer fiber strain rate of 0.01 min^{-1} while the initial outer fiber strain rate of tensile test is 0.1 min^{-1}.

The Izod impact strength with notching for all the composites are shown in Table 2 and Fig. 6. The impact strength of pure PP is 3.1 kJ m^{-2}. The fracture cross-section was examined using SEM and the micrographs are shown in Fig. 7a and b. The low magnification micrograph (Fig. 7a) indicates that the fracture initiated at a distance of about 300 μm from the notching line (the white arrow in Fig. 7a) and propagated outwards towards the surface of the sample. The fracture initiation point was the weakest point and failed first with concentrated stress. In the Izod impact test, the pendulum acts quickly on the notching side of the sample, resulting in a higher strain rate compared to the tensile test. At this high strain rate, the fracture morphology tends to be more brittle [56, 57]. Under this brittle fracture, the spherulitic morphology of PP can be easily observed on the surface (Fig. 7b). Addition of 6 wt% CNFs in the PP slightly decreased the impact strength to 3.0 kJ m^{-2}, which was not statistically significantly different from that of pure PP. The morphology of the fracture surface changed completely. Brittle and partial fibrillation was observed on the surface (Fig. 7c). The fracture initiation point is hard to estimate under this situation. Under the load applied by the pendulum, non-consistent motions between PP molecules and CNFs tend to create voids. With further deformation, void coalescence finally occurred, leading to the fibrillation failure at the interface of CNFs and PP. On the fracture surface shown in Fig. 7c, a large number of CNFs are exposed without any restriction. It appears that the bare CNFs simply lay on the top of polymer matrix. Simultaneously, the incompatibility between CNFs and PP created separate surfaces and voids originally in the composite, facilitating the debonding process between CNFs and PP under the load and leading to possible lower impact strength. The separated surfaces and holes between CNFs and polymer matrix can be easily observed in the higher magnification of fracture micrographs shown in Fig. 7d. However, well dispersed CNFs in PP are observed on the fracture micrographs of Fig. 7c. Addition of MAPP emulsion treated CNFs in PP did not change the impact strength significantly compared to pure PP and neat CNF-reinforced PP (Table 2). A previous study on CNF-reinforced PP showed serious degradation of impact strength with 6 wt% loading level [58]. In this study, the impact strength remained the same level with pure PP. Good dispersion of the dried CNFs in PP achieved using the masterbatch compounding process could be the main explanation for this observation. The fracture morphologies of PP+MAPP_CNF are shown in Fig. 7e and f. Good dispersion of MAPP_CNF was also observed. Similar to the sample of neat CNF-reinforced PP, brittle failure and a large amount of exposed CNFs are observed on the fracture surface. However, a close-up examination of fracture surface of the PP+MAPP_CNF nanocomposite indicates that some CNFs are partially bonded to the polymer matrix (Fig. 7f). MAPP emulsion treatment of the CNFs contributed to this apparent improved interfacial adhesion. In general, interfacial adhesion between reinforcements and matrix has a significant effect on composite impact strength [55]. Strong adhesion leads to high impact strength. In this case, however, only a very small amount of interfacial adhesion occurred the between the neat CNFs and PP and did not significantly increase the impact strength. The different particle size distributions of MAPP_CNFs and CNFs may also partially offset the effect of MAPP treatment. Modification of CNFs using MAPP pellet during the nanocomposite manufacturing process significantly increased the impact strength of PP from 3.1 to 3.8 kJ m^{-2}, which is about 23% higher than that of pure PP and 27% higher than neat CNF-reinforced PP. The cross-sectional fracture morphologies are shown in Fig. 8a–d. The fracture morphology in Fig. 8a indicated a brittle failure mode with no observable fracture initiation point [59], suggesting there may be no stress concentration point during the impact test and good dispersion of CNFs. A significantly lower amount of bare

 DOI 10.1002/pc

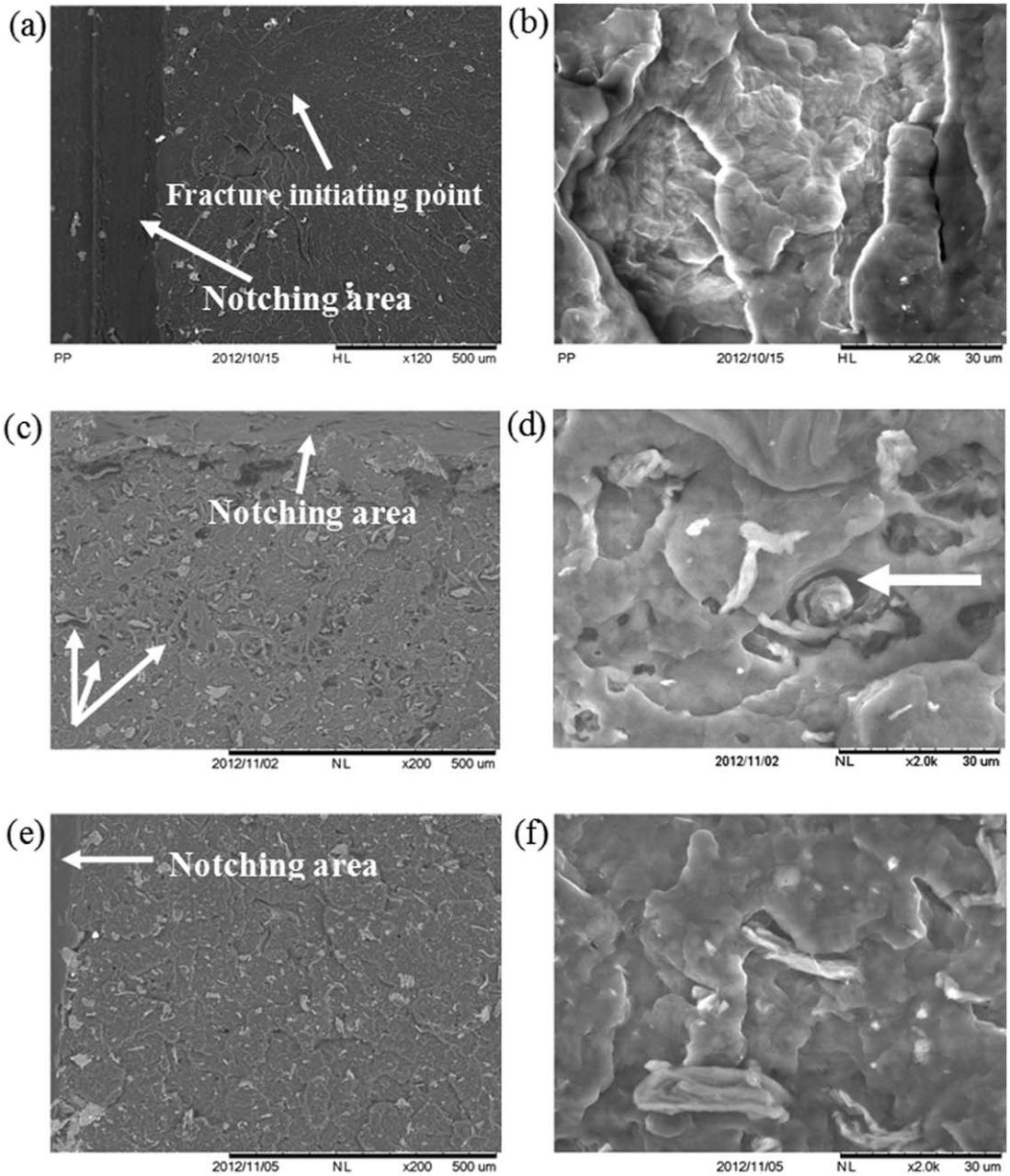

FIG. 7. Fracture cross-section of samples after impact tests. a and b: PP, c and d: PP+CNF, e and f: PP+MAPP_CNF.

CNFs are observed on the fracture surface when compared to that of neat CNF-reinforced PP. No separated surface and holes are observed. The higher magnification SEM micrographs shown in Fig. 8b–d indicate that strong interfacial adhesion was established between the polymer matrix, MAPP and the CNFs. After the impact test, splitting of the CNFs was also observed (Fig. 8b). Therefore, the impact strength of PP reinforced by MAPP pellet treated CNFs (PP+MAPP+CNF) was significantly improved when compared to the other CNF-PP nanocomposites.

The melt flow index data and its standard deviation of all the composites are also shown in Table 2. The MFI of PP after the extrusion process was 7.2 g/10 min. With the addition of 6 wt% of spray-dried CNFs into the PP, the nanocomposite showed a higher MFI value (8.7 g/10 min) compared with PP. Generally, the addition of natural fibers to polymer composites restricts molecular motion in the matrix and causes the lowering of MFI values [60, 61]. However, a slight increase of MFI value was observed in this case. One of the possibilities is the low loading level of CNFs used in the study. Second, phase separation between the CNFs and PP formed (the white arrow in the SEM micrographs of Fig. 7c and d) because of the incompatibility between the hydrophilic CNFs and hydrophobic PP. In addition, separation of PP molecules

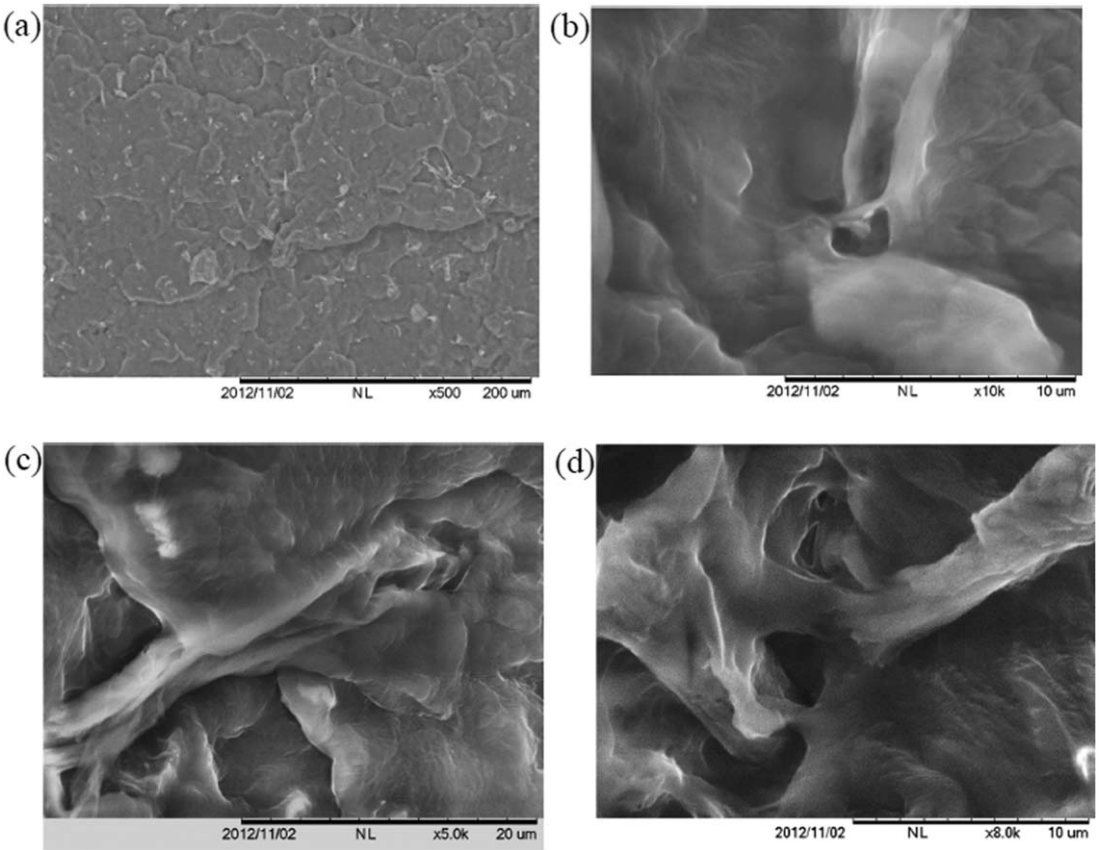

FIG. 8. Fracture cross-section of sample PP+MAPP+CNF after impact tests.

by the CNFs decreases the entanglement density of PP molecules, resulting in higher MFI values. Utilization of MAPP in the PP/CNFs system slightly decreased the MFI value compared to neat CNF-reinforced PP (Table 2). Compatibility between the CNFs and PP was improved using MAPP coupling agent, decreasing the amount of separate surfaces. Simultaneously, the stiffer CNFs limit the motion of PP molecules because of the established chain entanglement by MAPP, lowering the MFI values. However, the introduction of low molecular weight of MAPP lowered the composite viscosity (higher MFI values). The combination effect by introducing CNFs and MAPP into PP results in the nanocomposites having MFI values falling between the neat PP and neat CNF-reinforced PP. The modification on CNFs using MAPP pellets showed slightly lower MFI compared to the PP reinforced by MAPP emulsion treated CNFs. This may indicate that MAPP pellet treatment is more efficient in promoting chain entanglement between the CNFs and PP than that of MAPP emulsion treatment, which is consistent with the composite mechanical properties and morphological observations.

CONCLUSIONS

CNF suspension was dried using a laboratory scale spray-dryer and the spray-dried CNFs were then employed to reinforce PP using a two-step thermal compounding process. The PP based polymer nanocomposites with addition of CNFs (treated and untreated) exhibited higher tensile and flexural properties than those of pure PP. The highest mechanical properties were obtained for PP reinforced by MAPP pellet treated spray-dried CNFs. The tensile modulus, tensile strength, flexural modulus, and flexural strength of this nanocomposites were 1.94 GPa, 32.8 MPa, 1.63 GPa, and 50.1 MPa, which represents about 36, 11, 21, and 7% improvement compared to the respective properties of pure PP (1.43 GPa, 29.5 MPa, 1.35 GPa, and 46.9 MPa). This nanocomposite produced using PP, MAPP pellets, and spray-dried CNFs also showed the highest impact strength of 3.8 kJ m^{-2}. This value is about 23% higher than that of pure PP (3.1 kJ m^{-2}). Simultaneously, addition of neat CNFs and MAPP emulsion treated CNFs into PP sustained the impact strength of pure PP at this studied loading level. The fracture morphology examination of the impact tested samples indicates that good dispersion of CNFs in polymer matrix was achieved through the two-step thermal compounding process. MAPP treatments (either emulsion or pellet treatment) enhanced the interfacial adhesion between the CNFs and polymer matrix of PP. Based on this study, a provisional patent application [62] was filed for cellulose nanofibril polymer nanocomposites. Polymer nanocomposites using renewable nano materials is

feasible. Future study of polymer nanocomposites reinforced by spray-dried cellulose nanofibers are continuing with the manipulation of spray-drying process, fiber loading level, surface modification, etc.

ACKNOWLEDGMENTS

Much appreciation goes to The Process Development Center at the University of Maine for donating the nanofibrillated cellulose suspension.

REFERENCES

1. R. Kumari, H. Ito, M. Takatani, M. Uchiyama, and T. Okamoto, *J. Wood Sci.*, **53**, 470 (2007).
2. H. Yang and D.J. Gardner, *Wood Fiber Sci.*, **43**, 143 (2011).
3. Y. Peng, D.J. Gardner, and Y. Han, *Cellulose*, **19**, 91 (2012).
4. A. Amash and P. Zugenmaier, *Polymer*, **41**, 1589 (2000).
5. P. Wambua, J. Ivens, and I. Verpoest, *Comp. Sci. Technol.*, **63**, 1259 (2003).
6. J. Ganster, H.P. Fink, and M. Pinnow, *Comp. A*, **37**, 1796 (2006).
7. R. Gauthier, C. Joly, A.C. Coupas, H. Gauthier, and M. Escoubes, *Polym. Comp.*, **19**, 287 (1998).
8. A.K. Bledzki and J. Gassan, *Prog. Polym. Sci.*, **24**, 221 (1999).
9. H. Yang, H. Kim, J. Son, H. Park, B. Lee B, and T. Hwang, *Comp. Struct.*, **63**, 305 (2004).
10. N. Ljungberg, C. Bonini, F. Bortolussi, C. Boisson, L. Heux, and J.Y. Cavaillé, *Biomacromolecules*, **6**, 2732 (2005).
11. A. Dufresne, Nanocellulose: From Nature to High Performance Tailored Materials, Walter de Gruyter, Berlin, Germany (2012).
12. J.F. Beecher, *Nat. Nanotechnol.*, **2**, 466 (2007).
13. M.A. Hubbe, O.J. Rojas, L.A. Lucia, and M. Sain, *BioResources*, **3**, 929 (2008).
14. I. Siro and D. Plackett, *Cellulose*, **17**, 459 (2010).
15. Y. Habibi, L.A. Lucia, and O.J. Rojas, *Chem. Rev.*, **110**, 3479 (2010).
16. S.J. Eichhorn, A. Dufresne, M. Aranguren, N.E. Marcovich, J.R. Capadona, S.J. Rowan, C. Weder, W. Thielemans, M. Roman, S. Renneckar, W. Gindl, S. Veigel, J. Keckes, H. Yano, K. Abe, M. Nogi, A.N. Nakagaito, A. Mangalam, J. Simonsen, A.S. Benight, A. Bismarck, L.A. Berglund, and T. Peijs, *J. Mater. Sci.*, **45**, 1 (2010).
17. G. Siqueira, J. Bras, and A. Dufresne, *Polymers*, **2**, 728 (2010).
18. D. Klemm, F. Kramer, S. Moritz, T. Lindstrom, M. Ankerfors, D. Gray, and A. Dorris, *Angew. Chem. Int. Ed.*, **50**, 5438 (2011).
19. R.J. Moon, A. Marini, J. Nairn, J. Simonsen, and J. Youngblood, *Chem. Soc. Rev.*, **40**, 3941 (2011).
20. J. Bloch, Available at: http://umaine.edu/news/blog/2011/10/28/umaine-to-build-nation's-only-cellulose-nanofibrils-pilot-plant/ (Accessed Nov7, 2011).
21. W. Ferguson, *New Scientist*, **2878**, 24 (2012).
22. R. Wallace, Available at: http://blogs.usda.gov/2012/08/03/usda-under-secretary-sherman-unveils-nanocellulose-production-facility/(Accessed March 7, 2013).
23. Q. Yuan and R.D.K. Misra, *Polymer*, **47**, 4421 (2006).
24. S.M. Zebarjad, R. Bagheri, S.M. Seyed Reihani, and A. Lazzeri, *J. Appl. Polym. Sci.*, **90**, 3767 (2003).
25. S.M. Zebarjad, M. Tahani, and S.A. Sajjadi, *J. Mater. Process. Technol.*, **155/156**, 1459 (2004).
26. E. Qiu, T. Endo, and T. Hirotsu, *J. Appl. Polym. Sci.*, **94**, 1326 (2004).
27. W. Qiu, F. Zhang, T. Endo, and T. Hirotsu, *Polym. Compos.*, **26**, 448 (2005).
28. E. Bahar, N. Ucar, A. Onen, J. Wang, M. Oksüz, O. Ayaz, M. Ucar, and A. Demir, *J. Appl. Polym. Sci.*, **125**, 2882 (2012).
29. R. Andrews, D. Jacques, M. Minot, and T. Rantell, *Mater. Eng.*, **287**, 395 (2002).
30. D.J. Gardner, G.S. Oporto, R. Mills, and M.A.S.A. Samir, *J. Adhes. Sci. Technol.*, **22**, 545 (2008).
31. Y. Peng, D.J. Gardner, Y. Han, Z. Cai, and M.A. Tshabalala, *J. Colloid Interface Sci.*, **45**, 85 (2013).
32. W.J. Orts, J. Shey, S.H. Imam, G.M. Glenn, M.E. Guttman, and J. Revol, *J. Polym. Environ.*, **13**, 301 (2005).
33. F. Alloin, A. D'Aprea, A. Dufresne, N. El Kissi, and F. Bossard, *Cellulose*, **18**, 957 (2011).
34. A. Iwatake, M. Nogi, and H. Yano, *Compos. Sci. Technol.*, **68**, 2103 (2008).
35. L. Suryanegara, A.N. Nakagaito, and H. Yano, *Compos. Sci. Technol.*, **69**, 1187 (2009).
36. L. Suryanegara, H. Okumura, A.N. Nakagaito, and H. Yano, *Cellulose*, **18**, 689 (2011).
37. M. Jonoobi, J. Harun, A.P. Mathew, M.Z.B. Hussein, and K. Oksman, *Cellulose*, **17**, 299 (2010).
38. K. Oksman, A.P. Mathew, D. Bondeson, and I. Kvien, *Compos. Sci. Technol.*, **66**, 2776 (2006).
39. D. Bondeson and K. Oksman, *Compos. A*, **38**, 2486 (2007).
40. B. Wang and M. Sain, *Compos. Sci. Technol.*, **67**, 2521 (2007).
41. L. Jiang, E. Morelius, J. Zhang, M. Wolcott, and J. Holbery, *J. Compos. Mater.*, **42**, 2629 (2008).
42. K. Ben Azouz, E.C. Ramires, W. Van den Fonteyne, N. El Kissi, and A. Dufresne, *ACS Macro Lett.*, **1**, 236 (2012).
43. A.J. de Menezes, G. Siqueira, A.A.S. Curvelo, and A. Dufresne, *Polymer*, **50**, 4552 (2009).
44. A.L. Goffin, J.M. Raquez, E. Duquesne, G. Siqueira, Y. Habibi, and A. Dugresne, *Polymer*, **52**, 1532 (2011).
45. Y. Peng, Y. Han, and D.J. Gardner, *Wood Fiber Sci.*, **44**, 448 (2012).
46. M. Abdelmouleh, S. Boufi, M.N. Belgacem, A.P. Duarte, A. ben Salah, and A. Gandini, *Int. J. Adhes. Adhes.*, **24**, 43 (2004).
47. M.C.B. Salon, G. Gerbaud, M. Abdelmouleh, C. Bruzzese, S. Boufi, and M.N. Belgacem, *Magn. Reson. Chem.*, **45**, 473 (2007).
48. S. Berlioz, S. Molina-Boisseau, Y. Nishiyama, and L. Heux, *Biomacromolecules*, **10**, 2144 (2009).
49. P. Eronen, M. Österberg, and A.S. Jääskeläinen, *Cellulose*, **16**, 167 (2009).
50. K. Suzuki, A. Sato, H. Okumura, T. Hashimoto, A.N. Nakagaito, and H. Yano, *Cellulose*, **21**, 507 (2014).

51. W. Oraby, H.B. Hopfenberg, and V. Stannett, *J. Appl. Polym. Sci.*, **15**, 2987 (2003).

52. A. Arbelaiz, G. Cantero, B. Fernández, I. Mondragon, P. Gañán, and J.M. Kenny, *Polym. Compos.*, **26**, 324 (2005).

53. T.J. Keener, R.K. Stuart, and T.K. Brown, *Compos. A*, **35**, 357 (2004).

54. Y. Peng, D.J. Gardner, Y. Han, Z. Cai, and M.A. Tshabalala, *Cellulose*, **20**, 2379 (2013).

55. S. Fu, X. Feng, B. Lauke, and Y. Mai, *Compos. B*, **39**, 933 (2008).

56. A. Dasari, S. Sarang, and R.D.K. Misra, *Mater. Sci. Eng. A*, **368**, 191 (2004).

57. R.S. Hadal, A. Dasari, J. Rohrmann, and R.D.K. Misra, *Mater. Sci. Eng. A*, **372**, 296 (2004).

58. H. Yang, D.J. Gardner, and J.W. Nader, *Compos. A*, **42**, 2028 (2011).

59. H. Yang, D.J. Gardner, and J.W. Nader, *J. Appl. Polym. Sci.*, **128**, 3064 (2013).

60. N.J. Jam and A.H. Behravesh, *J. Thermoplast. Compos. Mater.*, **20**, 439 (2007).

61. D. Shumigin, E. Tarasova, A. Krumme, and P. Meier, *Mater. Sci.*, **17**, 32 (2011).

62. D.J. Gardner, Y. Han, and Y. Peng, Nanofibril-polymer composite, provisional U.S. patent application, PCT/US14/47100 (July 17, 2014).

 DOI 10.1002/pc